International Journal of Heat and Mass Transfer 52 (2009) 986–995

Contents lists available at ScienceDirect

International Journal of Heat and Mass Transfer

journal homepage: www.elsevier.com/locate/ijhmt

Experimental and theoretical studies of a two-stage pulse tube cryocooler operating down to 3 K

S. Kasthurirengan [a,*], G. Srinivasa [a], G.S. Karthik [a], D.S. Nadig [a], U. Behera [a], K.A. Shafi [b]

[a] Centre for Cryogenic Technology, Indian Institute of Science, Bangalore 560012, India
[b] T.K.M College of Engineering, Kollam, Kerala 691005, India

ARTICLE INFO

Article history:
Received 18 June 2007
Received in revised form 16 April 2008
Available online 18 September 2008

Keywords:
Pulse tube
Cryocooler
Regenerator
Helium
Refrigeration
Numerical modeling

ABSTRACT

The development of a two-stage Pulse Tube Cryocooler (PTC) which produces a no-load temperature of ~3 K and delivers a refrigeration power of ~250 mW at 5 K is reported in this work. The system uses stainless steel meshes along with lead (Pb) granules and combinations of Pb, Er_3Ni and $HoCu_2$ in layered structures as the first and second stage regenerator materials respectively. With Helium as a working fluid, the pressure oscillations are generated using a 6 kW water-cooled Helium compressor along with an indigenous rotary valve. Different configurations of pulse tube systems have been experimentally studied, by both varying the dimensions of pulse tubes and regenerators as well as the second stage regenerator material composition. The pulse tube Cryocooler has been numerically analyzed by using both the isothermal model and the model based on solving the energy equations. The predicted refrigeration powers as well as the temperature profiles have been compared with the experimental results for specific pulse tube configurations.

1. Introduction

In the recent years, for several applications such as cooling of sensors, superconducting magnets, cryopumping etc, there are worldwide efforts to replace cooling with liquid helium by cooling with closed cycle cryocoolers. This is because of both the shortage of liquid helium supply and the availability of efficient, highly reliable cryocoolers as on date, and due to the significant developments in cryocoolers such as Gifford McMahon (GM), Stirling and Pulse tube, etc. over the last few decades. Of these, Pulse tube Cryocoolers (PTC) offer specific advantages such as lower vibration levels, higher reliability for long term performance by the absence of moving parts at cryogenic temperatures.

Since the discovery of basic PTC by Gifford and Longsworth [1], essential improvements of this cooler have been achieved by the addition of a buffer volume and an orifice to produce the phase shift between mass flow rate and pressure of the working fluid (known as orifice PTC) [2,3]. A further significant improvement resulted by the addition of a second orifice in between the Pulse tube warm end and the main gas inlet [4] (called double inlet PTC). This second inlet reduces the mass flow through the regenerator and acts as an additional phase shifter resulting in the lowest no load temperature of single stage system near 30 K [5].

Achieving temperatures in the liquid helium range called for a staging design. Further, rare earth compounds such as Er_3Ni, $HoCu_2$, which exhibit increased specific heats (due to magnetic phase transitions) at temperatures around 10 K are used as regenerator materials in the second stage, to match the specific heat of helium gas at these temperatures [6]. The volumetric specific heats of some of the commonly used regenerator materials along with that of helium are given in reference [7]. A temperature of 3.6 K was obtained by Matsubara and Gao [8] with a three-stage system, while with a liquid nitrogen pre-cooled two-stage system, a temperature of 2.07 K was obtained by Thummes et al [9]. Wang et al [10] could achieve a lowest temperature of 2.23 K in a two stage PTC along with a refrigeration power of ~370 mW at 4.2 K using a three layer regenerator filled with $ErNi_{.9}Co_{.1}$, ErNi and Pb.

Since then, research has been continued in this field [11–14] and with the developments over the years, now commercial PTCs are available [15,16] for various applications. In spite of this, the research works in this field are quite active to understand the fundamental cooling mechanisms in PTCs to achieve further technological breakthroughs.

This paper discusses the design and development of a two stage pulse tube Cryocooler, which produces a no-load temperature of ~ 3 K and provides a refrigeration power of 250 mW at 5 K. Experimental studies of different pulse tube configurations have been conducted by varying the dimensions of the pulse tubes and regenerators to arrive at the best one, which leads to the lowest temperature. Using this configuration, experimental studies

* Corresponding author. Tel./fax: +91 80 23601612.
E-mail addresses: kas@ccf.iisc.ernet.in, chairman@ccf.iisc.ernet.in (S. Kasthurirengan).

0017-9310/$ - see front matter © 2008 Elsevier Ltd. All rights reserved.
doi:10.1016/j.ijheatmasstransfer.2008.07.028

Nomenclature

A	area (m^2)
A_0	area of orifice (m^2)
A_{CX2}^{outer}	outer surface area of second stage cold end (m^2)
A_m	cross section area of the medium (m^2)
A_{flow}	area of flow (m^2)
A_{HT}	heat transfer area (m^2)
C_p	specific heat of gas at constant pressure (J/(kg K))
C_r	heat capacity ratio (dimensionless)
C_w	volumetric specific heat of regenerator materials (J/(m^3 K))
d_{RG}	diameter of the regenerator (m)
d_h	equivalent or hydraulic diameter (m)
d_s	average diameter of spherical particle in matrix (m)
dT/dx	temperature gradient along the length dx (K/m)
e_c	emissivity of the cold surface (dimensionless)
e_h	emissivity of the hot surface (dimensionless)
e_s	emissivity of the radiation shields (dimensionless)
f	friction factor (dimensionless)
F	view factor (dimensionless)
G	mass flow rate per unit area (kg/(s m^2))
h	specific enthalpy (J/kg)
$\dot{h}_{RG}$	enthalpy flow rate through regenerator (W)
$\dot{h}_{PT}$	enthalpy flow rate through pulse tube (W)
I_{RG}	regenerator ineffectiveness (dimensionless)
ε_{RG}	regenerator effectiveness (dimensionless)
k	thermal conductivity of gas (W/(m K))
k_m	thermal conductivity of the medium (W/(m K))
l_{RG}	length of the regenerator (m)
M, m	mass (kg)
m_w	mass of regenerator materials (kg)
$\dot{m}$	mass flow rate (kg/s)
$\dot{m}_c$	mass flow rate at the cold end (kg/s)
$\dot{m}_{RG}$	mass flow rate through the regenerator (kg/s)
$\dot{m}_o$	mass flow rate through the orifice or double inlet valve (kg/s)
NTU	number of heat transfer units
N_s	number of radiation shields (dimensionless)
P	pressure (Pa)
P_{avg}	average pressure (Pa)
P_l	pressure at the left end (Pa)
P_r	pressure at the right end (Pa)
ΔP	pressure drop (Pa)
Pr	Prandtl Number (dimensionless)
PR	pressure ratio (dimensionless)
Q_a	actual theoretical refrigeration power (W)
Q_{exp}	experimentally measured refrigeration power (W)
Q_i	ideal theoretical refrigeration power (W)
Q_{AC}	refrigeration loss due to axial conduction (W)
Q_{loss}	refrigeration loss due to a given mechanism (W)
Q_{RG}	refrigeration loss due to regenerator ineffectiveness (W)
Q_{pd}	refrigeration loss due to pressure drop in regenerator (W)
Q_{rad}	refrigeration loss due to radiation from ambient (W)
R	gas constant per unit mass (kJ/kg K)
Re	Reynolds Number (dimensionless)
T	temperature (K)
T_0	ambient temperature (K)
T_h, T_c	hot and cold boundary temperatures (K)
T_{R1}	average temperature of 1st stage regenerator (K)
T_{R2}	average temperature of 2nd stage regenerator (K)
T_{CX1}	cold end temperature of 1st stage (K)
T_{CX2}	cold end temperature of 2nd stage (K)
T_i	temperature of the ith element (K)
T_{wi}	temperature of the wall at ith element (K)
t	time (s)
Δt	time interval (s)
u	specific internal energy (J/kg)
v	flow velocity (m/s)
V	volume (m^3)
V_{I1},V_{I2}	volumes of section I of the 1st, 2nd stage Pulse tubes (m^3)
V_{II1},V_{II2}	volumes of section II of the 1st, 2nd stage Pulse tubes (m^3)
V_{III1},V_{III2}	volumes of section III of the 1st, 2nd stage Pulse tubes (m^3)
V_{CX1}	volume of the first stage cold end heat exchanger (m^3)
V_{CX2}	volume of the second stage cold end heat exchanger (m^3)
V_{CR}	volume of Compressor cylinder (m^3)
V_{PT}	volume of the pulse tube (m^3)
V_{RX}	volume of the ambient heat exchanger above 1st stage Regenerator (m^3)
V_{R1}	volume of the first stage regenerator (m^3)
V_{R2}	volume of the second stage regenerator (m^3)

Greek letters

α	heat transfer coefficient (W/(m^2 K))
σ	Stefan–Boltzmann constant ($\sigma = 5.67 \times 10^{-8}$ W/(m^2 K^4))
v	specific volume (m^3/kg)
γ	ratio of specific heats ($\gamma = C_p/C_v$) (dimensionless)
η	viscosity (Pa s)
τ	time period of pressure oscillation (s)
φ	porosity (dimensionless)
Γ, Γ^*	temperature Distributions

Subscripts

h	hot end
c	cold end
a	ambient
RG	regenerator
PT	pulse tube
i, j, n	space element, space element boundary, and time element indices

have also been conducted by varying the composition of the second stage regenerator materials. Although the current refrigeration powers of the developed pulse tube cryocooler is lower than that of commercial pulse tube cryocoolers, the detailed experimental studies on different configurations on two stage PTCs will provide valuable technical information towards their design.

Theoretical understanding of the fundamental cooling mechanisms in PTCs has been attempted by several authors by using different models [17–23]. Of these, we have adopted two models for our analysis. The first is the isothermal model developed by Zhu and Chen [19], which assumes the working fluid to be an ideal gas. The second model is that developed by Wang [20,22] which solves the energy equation of the working fluid (Helium) in the pulse tube / regenerator system after taking into account its real gas properties. The theoretical predictions of these numerical models are compared with the experimental results for specific pulse tube configurations.

2. Experimental setup and details

Fig. 1 shows the schematic of the two-stage PTC. In this configuration, the cold end of the first stage regenerator forms the warm end of the second stage regenerator. The pulse tubes of both the stages are mounted separately at their warm ends on the base

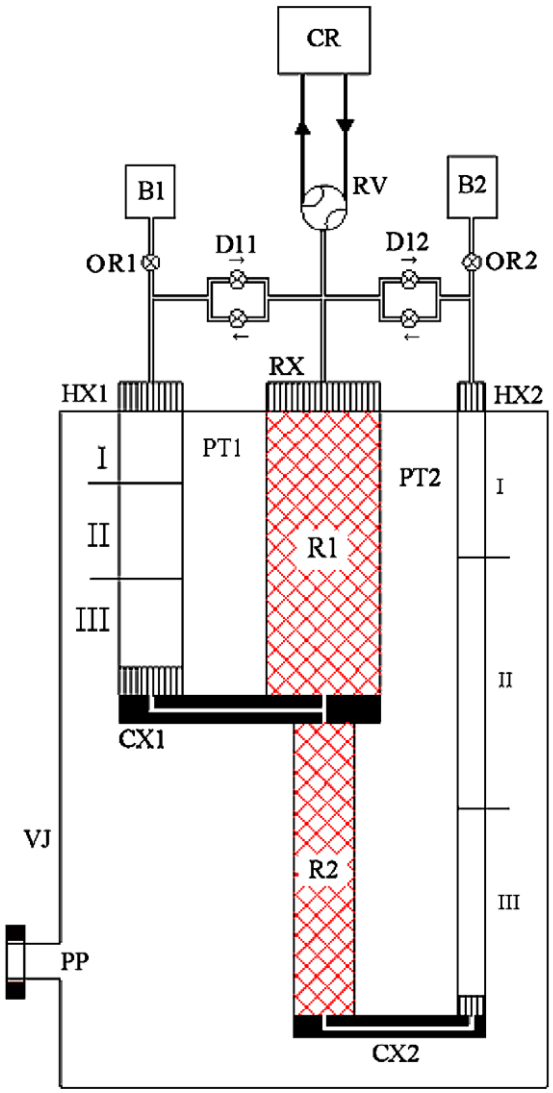

Fig. 1. Schematic of the two stage Pulse tube Cryocooler, HX – Heat exchanger at the Pulse tube hot end, CX – Heat exchanger at the Pulse tube cold end, RX – Heat exchanger at the regenerator hot end, DI – Double-inlet valve, OR – Orifice valve, RV – Rotary valve, B – Buffer volume, CR – Compressor, PP – Evacuation port, VJ – Vacuum jacket, PT – Pulse tube, R – Regenerator. Numbers '1' and '2' in the schematic correspond to the respective components at 1st stage and the 2nd stage in the system.

stainless steel flange. The pulse tube and regenerator housings are made of thin walled stainless steel tubes (wall thickness ~0.5 mm) and end in flanged construction. Different configurations of the PTCs have been built by varying dimensions of pulse tubes and the regenerators and these details are presented in the later part of this paper.

The first stage regenerator is fabricated in most cases with stainless steel meshes (mesh size = 200) along with Pb (average grain size ~250 μm) to about 15% by volume towards the cold end. However, for some specific experiments, this regenerator is fabricated entirely with stainless steel meshes. On the other hand, combinations of Pb, Er_3Ni and $HoCu_2$ (average grain size ~250 μm) from warm end to cold end in layered structures with different volume percentage ratios have been used as the second stage regenerator materials. The system uses buffer volumes of 1 litre and 0.5 litre for the first and second stages respectively. These are connected to the hot ends of pulse tubes of corresponding stages through the respective orifice valves as shown in Fig. 1. Needle valves (Swagelok, M-series) are used as orifice (OR) and anti-parallelly arranged double inlet (DI) valves to create the necessary phase shifts. All the room temperature seals are made with neoprene o-rings, while the low temperature seals are made with indium.

The heat exchangers at the warm and cold ends are fabricated from electrolytic grade copper. Both slit type and hole type heat exchangers have been experimented in our studies and it is observed that the former types performed better than the latter. Heat dissipation at the warm end heat exchangers to ambient is accomplished by convective cooling by the finned structures at their outer surfaces. The temperatures of the first stage cold end and at different locations on the pulse tubes and regenerators are measured using platinum resistance thermometers (PT500). The temperature of the second stage cold end is measured by precalibrated silicon diode sensors (Lakeshore, model DT470 and Scientific Instruments, model SI410).

Fig. 2 shows the photograph of instrumented cold end of the two-stage PTC. The second stage cold end is initially wrapped with a few layers of superinsulation (Aluminized Mylar+Nylon net spacers) and enclosed within the radiation shield (made of Aluminum) clamped to the first stage. Subsequently, this radiation shield, the first stage pulse tube and the regenerator are insulated with ~10 layers of superinsulation and mounted within a stainless steel jacket and evacuated by a vacuum pumping system to pressures $<10^{-3}$ mbar, before the start of cooldown.

A 6kW water-cooled helium compressor (Leybold, model Coolpak 6000) serves as the pressure source. This is used with an indigenous rotary valve to generate the pressure oscillations. The frequency of the pressure waveform can be varied by using an inverter drive (Integrated systems, model INVAC). The pressure waveform at the inlet of the first stage regenerator and the warm

Fig. 2. Photograph of the two-stage Pulse tube system.

ends of the first and second stage pulse tubes are monitored by pressure transducers (Siemens, model KPY47). Data acquisition of the various parameters such as temperatures and pressures are carried out using a LabVIEW based program along with IEEE interface and a system controller.

3. Experimental results

3.1. Pressure waveforms

The typical pressure waveforms at the inlet of the first stage regenerator and at the warm ends of the first and second stage Pulse tubes at the operating frequency of 1.6 Hz are shown in Fig. 3. The shape of these waveforms lies in between sinusoidal and trapezoidal forms. This experimentally measured pressure waveforms are used as the input data in the theoretical analysis of numerical models to be discussed later.

3.2. Cool down behavior

Table 1 shows the details of the several pulse tube configurations experimentally studied along with the lowest temperature achieved in their first and second stages. The cool down behaviour of the first and second stage cold ends of PTC for the best configuration (i.e. the one with the lowest temperature and No.7 in Table 1) is shown in Fig. 4. Typically, ~180 min is required for the second stage cold end to reach below 4 K.

3.3. Refrigeration power characteristics

The refrigeration power characteristics of pulse tube cryocoolers are measured by applying electrical power to a Manganin heater (of resistance ~30 ohms) wound on the cold end heat exchanger and measuring the steady temperatures reached. The refrigeration power characteristics of the second stage of the PTC configurations 1 to 7 are shown in Fig. 5. The configuration 7 which has the lowest no-load temperature of ~3 K gives a refrigeration power of ~250 mW at 5 K. However, the performance of this configuration is poor at heat loads greater than 2 W, when compared to those of 2, 3 and 4. The latter configurations provide a refrigeration power of nearly 5 W around 27 K.

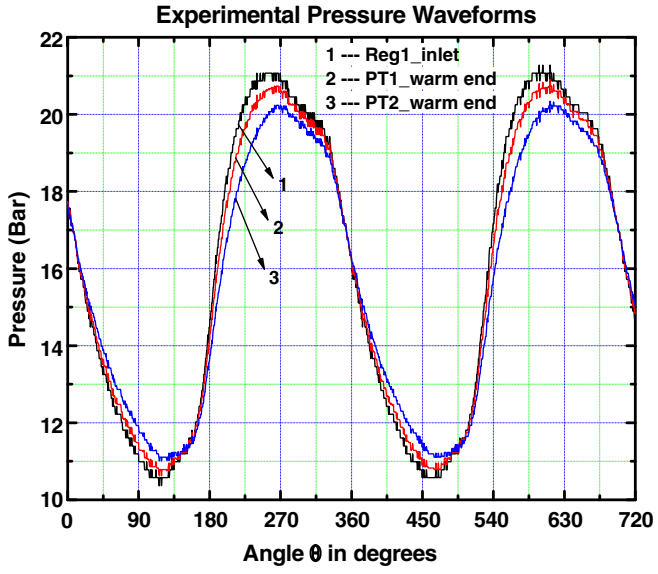

Fig. 3. Pressure waveforms at the inlet of the first stage regenerator and warm ends of the first and second stage pulse tubes.

The measured refrigeration powers of our pulse tube systems are quite comparable with those reported in the literature on nearly similar pulse tube configurations, with lead as the second stage regenerator material. Such a comparison is also shown in Fig. 5. Wang et al [24] report a minimum temperature of 11.5 K and a refrigeration power of ~1.3 W at 20 K. On the other hand, Wild et al [25] report a minimum temperature of 11 K and a refrigeration power of ~2 W at 18 K.

3.4. Effect of dimensions of pulse tube and regenerators on the cold end temperatures

In our experimental studies, the materials and the methods used for the fabrication of pulse tubes and regenerators of different dimensions are kept same. Since the design of the cold end and warm end heat exchangers for different configurations and other components which are mounted at ambient are identical, this enables the comparison of different PTC configurations to obtain qualitative understanding of the effect of dimensional changes on the cold end temperatures. The following are some of the observations from our experimental studies.

(a) *First stage pulse tube*. The effect of first stage pulse tube length on its cold end temperature appears to be significant. This can be seen by comparing the configurations 4 and 5. Increasing the pulse tube length by 70 mm leads to a decrease in the first stage temperature from 73.8 K to 59.9 K. Comparison of the configurations 1 and 2 shows that the diameter of the first stage pulse tube also has a significant effect on its cold end temperature. A change in the pulse tube diameter from 14 mm to 19 mm has led to the decrease of first stage cold end temperature from 118.4 K to 86.3 K.

(b) *First stage regenerator*. The effect of the first stage regenerator length on its cold end temperature appears to be less. This can be seen by comparing the configurations 11 and 12. Although the length of the regenerator is increased by 37 mm the first stage cold end temperature drops only by 4.4 K. Comparison of configurations 12 and 15 shows that the effect of diameter of the first stage regenerator is less on its cold end temperature. A change in the regenerator diameter from 25 mm to 19 mm leads to an increase of the first stage temperature by 4 K.

(c) *Second stage pulse tube*. The effect of second stage pulse tube length on its cold end temperature is significant, which can be seen by comparing the configurations 11 and 13. Decrease in the pulse tube length from 390 mm to 350 mm leads to a decrease in the second stage cold end temperature from 6.5 K to 4.5 K. Similarly, the comparison of the configurations 9 and 10 shows that the diameter of the second stage pulse tube has a significant effect on its cold end temperature. Decrease of the second stage pulse tube diameter from 14 mm to 10 mm causes an increase in the second stage cold end temperature from 24.4 K to 59.5 K.

(d) *Second stage regenerator*. The effect of second stage regenerator length on its cold end temperature appears to be less. A comparison of the configurations 12 and 14 shows that increasing the regenerator length by 40 mm leads to a marginal increase of the cold end temperature from 4.5 K to 4.7 K. Similarly a comparison of the configurations 1 and 8 shows that the diameter of the second stage regenerator has less effect on its cold end temperature. A change in the regenerator diameter from 19 mm to 25 mm leads to an increase in the second stage cold end temperature from 13.5 K to 14 K.

Table 1
Details of experimental pulse tube configurations

Sl No	1st stage				2nd stage				Regenerator materials		No load temperature (K)	
	PT		Reg		PT		Reg					
	D	L	D	L	D	L	D	L	1st stage	2nd stage	1st stage	2nd stage
1	14	200	25	163	14	350	19	190	SS + Lead (85% + 15%)	Lead + SS (85% + 15%)	118.4	13.5
2	19	200	25	163	14	350	19	190	SS + Lead (85% + 15%)	Er_3Ni + Lead + SS (31% + 57% + 12%)	86.3	7.8
3	19	200	38	140	14	350	19	190	SS (100%)	Er_3Ni + Lead + SS (31% + 57% + 12%)	80.0	7.2
4	19	200	25	200	14	390	19	190	SS + Lead (85% + 15%)	Er_3Ni + SS (85% + 15%)	73.8	5.1
5	19	270	25	200	14	390	19	190	SS + Lead (85% + 15%)	Er_3Ni + Lead + SS (31.5% + 57% + 11.5%)	59.9	3.5
6	19	270	25	200	14	390	19	190	SS + Lead (85% + 15%)	$HoCu_2$ + Lead + SS (30% + 40% + 30%)	65.0	3.3
7	19	270	25	200	14	390	19	190	SS + Lead (85% + 15%)	$HoCu_2$ + Er_3Ni + Lead + SS (27% + 27% + 27% + 19%)	66.7	3.0
8	14	200	25	163	14	350	25	190	SS + Lead (85% + 15%)	Er_3Ni + Lead + SS (37% + 27% + 36%)	118.7	14.0
9	25	150	38	140	14	350	19	190	SS (100%)	Er_3Ni + Lead + SS (31% + 57% + 12%)	176.5	24.4
10	25	150	38	140	10	350	19	190	SS (100%)	Er_3Ni + Lead + SS (31% + 57% + 12%)	188.9	59.5
11	19	270	25	163	14	390	19	190	SS + Lead (85% + 15%)	Er_3Ni + Lead + SS (31% + 57% + 12%)	76.4	6.5
12	19	270	25	200	14	390	19	190	SS + Lead (85% + 15%)	Er_3Ni + Lead + SS (31% + 57% + 12%)	72.0	4.5
13	19	270	25	163	14	350	19	190	SS + Lead (85% + 15%)	Er_3Ni + Lead + SS (31% + 57% + 12%)	77.0	4.5
14	19	270	25	200	14	390	19	230	SS + Lead (85% + 15%)	Er_3Ni + Lead + SS (31% + 57% + 12%)	70.0	4.7
15	19	270	19	200	14	390	19	190	SS + Lead (85% + 15%)	Er_3Ni + Lead + SS (31% + 57% + 12%)	76.0	4.6

PT – Pulse tube, Reg – Regenerator, D – Diameter, L – Length, SS – Stainless Steel meshes (size 200). All dimensions are in mm.

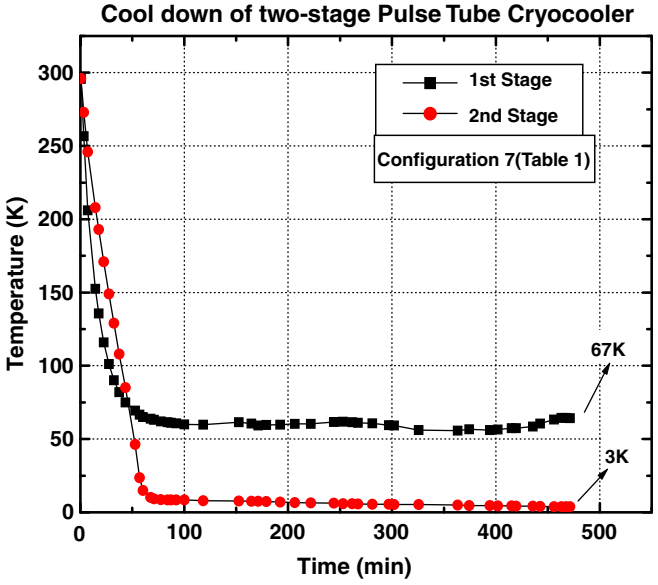

Fig. 4. Typical cool down of the two-stage Pulse tube system.

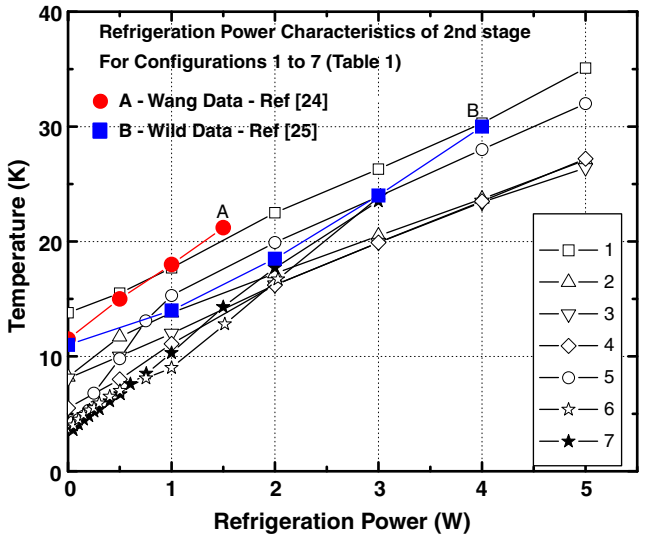

Fig. 5. Refrigeration power characteristics of some of the Pulse tube configurations (in Table 1). The data from references [24] and [25] are also included in the same graph.

From the above observations it can be inferred that the changes in dimensions of the pulse tubes have significant effect on their cold end temperatures compared to the changes in those of the regenerators.

3.5. Effect of regenerator materials on the second stage cold end temperature

Experimental studies clearly indicate the need for magnetic materials such as Er_3Ni, $HoCu_2$ for second stage regenerator to achieve temperatures below 10 K. As can be seen from Table 1, the temperature of $\sim$ 3 K is obtained for configuration 7 with regenerator materials Er_3Ni, $HoCu_2$, Pb and Stainless steel meshes in the volume percentage ratio 27:27:27:19. Also detailed experiments were conducted by varying the volume percentage ratios of Er_3Ni to Pb and $HoCu_2$ to Pb, while keeping the dimensions of the PTC system same as that of configuration 7.

Fig. 6 plots the second stage cold end temperature as a function of the percentage ratio of $HoCu_2$ to Pb for different refrigeration powers. It is obvious that even using 20% $HoCu_2$ vs Pb leads to significant lowering of cold end temperature. For lower refrigeration powers, increasing the percentage of $HoCu_2$ vs Pb does not significantly decrease cold end temperature further. But for higher refrigeration powers, the cold end temperature oscillates with increasing percentage of $HoCu_2$ vs Pb. Experiments indicate that the optimum ratio of $HoCu_2$ to Pb should be of the order of 2:3.

Similar results are shown in Fig. 6 for the combination of Er_3Ni and Pb. It is seen that the use of Er_3Ni along with Pb leads to a decrease in the cold end temperature. However, this effect is not so significant as in the case of $HoCu_2$ with Pb. The optimum ratio of Er_3Ni to Pb should be of the order of 3:2. Further increase in this ratio leads to only poor performance at all refrigeration powers.

4. Modeling of the pulse tube system

The theoretical analysis of the pulse tube system has been carried out using two independent models. The first one is the isothermal model in one dimension, which assumes ideal gas properties of the working fluid. This model originally developed by Zhu et al. [19] for a single stage PTC, has been extended to two-stage

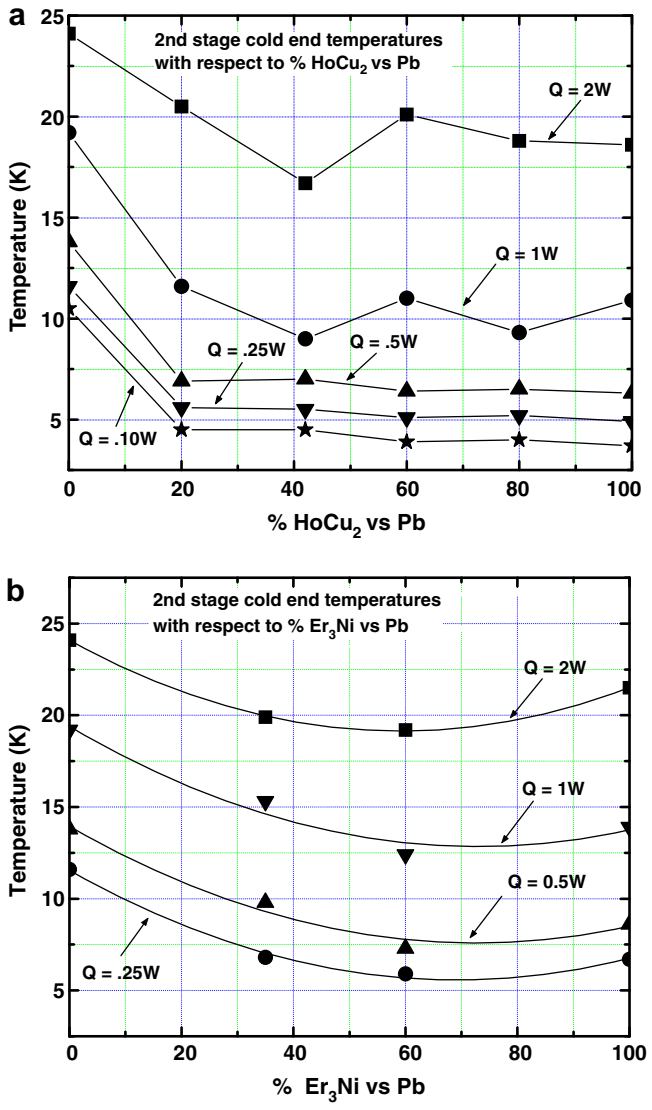

Fig. 6. (a) Plot of second stage cold end temperatures as a function of percentage ratio of $HoCu_2$ vs Pb for different refrigeration powers. (b) Plot of second stage cold end temperatures as a function of percentage ratio of Er_3Ni vs Pb for different refrigeration powers.

PTCs. The second is the model developed by Wang [20,22], which is also in one dimension, solves the energy equation by finite difference techniques, but takes care of the real gas properties of the working fluid. They are briefly described below.

4.1. The isothermal model

In this model developed by Zhu et al [19] for single stage PTCs, the gas in the pulse tube is divided into three parts as shown in Fig. 1. It is assumed that the gas in Sections 1 and 3 undergo isothermal processes, while that in Section 2 undergoes an adiabatic process during the application of the pressure waveform. By extending the equations developed by Zhu et al for the two-stage PTC, the total mass M from the compressor upto volume *III* in both the stages is given by the following equation.

$$P\left(\frac{V_{CR}}{RT_o}+\frac{V_{RX}}{RT_o}+\frac{V_{R1}}{RT_{R1}}+\frac{V_{CX1}}{RT_{CX1}}+\frac{V_{III1}}{RT_{CX1}}+\frac{V_{R2}}{RT_{R2}}+\frac{V_{CX2}}{RT_{CX2}}+\frac{V_{III2}}{RT_{CX2}}\right) = M \quad (1)$$

In our analysis, the volume variation of V_{CR} is obtained by matching the experimentally measured pressure waveform at the inlet of the first stage regenerator. The average temperatures of the regenerators T_{R1} and T_{R2} are chosen as the logarithmic mean values of their end temperatures due to the nonlinear temperature profiles across them. An iterative procedure is used to obtain consistent values for the total mass M, for given values of V_{III1} and V_{III2}.

Since both the stages are similar, the equations relating to the mass flow rates through their orifice and double inlet valves are also similar. Hence in the following equations, the subscripts 1 and 2 which refer to the respective stages have been omitted. The mass flow rate through the orifice or the double inlet valve is given by,

$$\dot{m}_o = A_o\sqrt{\left(\frac{2\gamma}{(\gamma-1)}\frac{P_l}{v}\left(\left[\frac{P_r}{P_l}\right]^{\frac{2}{\gamma}}-\left[\frac{P_r}{P_l}\right]^{\frac{\gamma+1}{\gamma}}\right)\right)} \quad \text{when } P_l > P_r \quad (2a)$$

$$\dot{m}_o = -A_o\sqrt{\left(\frac{2\gamma}{(\gamma-1)}\frac{P_r}{v}\left(\left[\frac{P_l}{P_r}\right]^{\frac{2}{\gamma}}-\left[\frac{P_l}{P_r}\right]^{\frac{\gamma+1}{\gamma}}\right)\right)} \quad \text{when } P_l < P_r \quad (2b)$$

Here, P_l and P_r represent the pressure on the left and right ends of the valve. If the mass flow rate from left to right is taken as positive, the mass flow rate from right to left will be negative and hence the negative sign in the Eq. (2b). In general, it is assumed that the mass flow rate is positive when the gas flows from the compressor into the pulse tube through the regenerator. The gas flow through the double inlet valve is caused by the pressure drop across the regenerators and hence the experimentally measured pressure waveforms at the inlet of the first stage regenerator and the outlet of the first and second stage pulse tubes are used as input data in the calculations.

The orifice area A_o is determined using the data sheets from the manufacturer on the valve dimensions and the relation between the flow coefficient and the number of turns of orifice opening. For the Swagelok M series type metering valves used in our experimental setup, the orifice area is 1.58 mm^2 when the valve is fully open.

Following the procedures outlined by Zhu et al [19], with the boundary condition that $V_{PT} = V_I + V_{II} + V_{III}$, convergent values of V_I, V_{II} and V_{III} for the respective stages are obtained. The gas in the volume V_{III2} moves in and out of the cold end heat exchanger of the second stage of the Pulse tube and hence the refrigeration power of this stage is given by,

$$Q_i = \frac{1}{\tau}\int_0^{\tau} PdV_{III} \quad (3)$$

Since the variations of both P and V_{III2} with time are known, Q_i can be calculated. This corresponds to the ideal refrigeration power without any losses. When the losses of refrigeration power by various mechanisms are subtracted from Q_i, one obtains Q_a, which refers to the actual refrigeration power, estimated theoretically. A comparison of Q_a with the experimentally measured refrigeration power Q_{exp} is presented in a later section.

4.2. The energy equation model

This one dimensional numerical model is that developed by Wang [20], and assumes (a) real gas properties of the working fluid, helium, (b) constant temperatures of cold and warm end heat exchangers, (c) no axial conduction. The governing equations along with the solving methodology are described in reference [22]. However, for the sake of continuity in reading, they are briefly described below.

Since our focus is on the second stage pulse tube and its regenerator, only these components are chosen for our analysis as shown in Fig. 7. Thus, the left boundary is the first stage cold

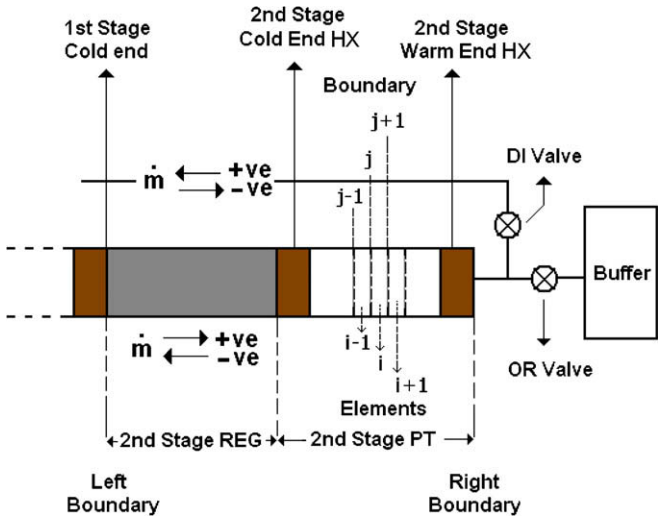

Fig. 7. Discretization of Pulse tube / regenerator for energy equation model. Here 'HX' represents heat exchanger, 'OR' represents the orifice and 'DI' represents Double Inlet, 'i' represents the elemental control volume, and 'j' represents its left boundary.

end, while the right boundary is the warm end of the second stage pulse tube. The pulse tube and the regenerator are divided into a number of discrete volume elements as shown in the Fig. 7. Here, i represents the element and j represents its left boundary. The discretized form of energy equation for the pulse tube / regenerator is given by,

$$\frac{(mh-PV)_i-(mh-PV)_i^{n-1}}{\Delta t}+(\dot{m}h)_{j+1}-(\dot{m}h)_j+\alpha A_i(T_i-T_{wi})+P\frac{V_i-V_i^{n-1}}{\Delta t}=0$$

The discretized form of energy equation for regenerator materials is given by,

$$m_{wi}\frac{(C_{wi}T_{wi}-C_{wi}^{n-1}T_{wi}^{n-1})}{\Delta t}=\alpha A_i(T_i-T_{wi}) \quad (5)$$

Similarly, the discretized form of continuity equation is given by,

$$\frac{m_i-m_i^{n-1}}{\Delta t}=\dot{m}_{j+1}-\dot{m}_j \quad (6)$$

The superscript $(n-1)$ refers to the variables at the $(n-1)^{th}$ time interval and those without the superscript refer to those at n^{th} time interval. The mass flow rates of the elements are obtained by using the continuity equation. The mass flow rate through the right boundary of the total system is that through the orifice and double inlet valves and is given by Eqs. (2a) and (2b). The real gas properties such as h and u are obtained using NIST12 helium database.

The second order upwind difference method is applied to the convection terms in Eq. (4). The above equations are solved by using Tri-Diagonal Matrix Algorithm (TDMA) method, with the assumption of an initial temperature distribution Γ in the pulse tube and the regenerator system along with end boundary conditions. The actual pressure waveform serves as an input in the calculations. A new temperature profile Γ^* (i.e. temperatures at all nodal points) is obtained as a solution of the above equations. This serves as the initial temperature distribution Γ for the next iteration. These iterations are performed until the difference between Γ and Γ^* becomes negligible.

The temperature T_i^n for the element i at the time step n is obtained from that at time $(n-1)$, using the relation

$$T_i^n=T_i^{n-1}(P^n/P^{n-1})^{(\gamma-1)/\gamma} \quad (7)$$

Subsequently, the above calculations are continued for the next time step. The procedure is continued till the cycle is completed and convergence is obtained.

The refrigeration power of the pulse tube Cryocooler is the difference between the enthalpy flow rate through the pulse tube and that through the regenerator. For a perfect regenerator, this enthalpy flow rate is zero. Hence, this model already accounts for the losses through the regenerator in the calculation of the refrigeration power. The calculated refrigeration powers using the above equation are compared with the actual experimental data in a later section.

4.3. Refrigeration power losses

The losses of refrigeration power [26–29] result by several mechanisms such as (a) Axial conduction, (b) Regenerator ineffectiveness, (c) Pressure drop in the regenerator, (d) Radiation to Pulse tube Cold end from ambient, (e) Gas conduction in the vacuum jacket etc. Of these, the loss due to gas conduction is quite small, because of cryopumping effects at very low temperatures and can be neglected. Hence, in our analysis, only the other losses have been evaluated and taken into account. They are described briefly below.

4.3.1. Axial conduction

The heat transfer by axial conduction is an important mechanism for the loss of refrigeration power. In a pulse tube, the axial heat conduction takes place through its walls and helium gas, while in a regenerator, this occurs through the wall, helium gas in the void volume and the matrix material filled within. Ju [27] has shown that the sinusoidal oscillations of gas flow at high pressure in the pulse tube and regenerator lead to enhanced heat conduction at a rate an order of magnitude greater than the pure gas conduction. Thus the effective heat conduction losses due to helium gas, solid wall and regenerator matrix may be of the same order of magnitude.

The conduction heat flow Q_{AC} across a small section of length dx in a medium is given by

$$Q_{AC}=k_mA_m(dT/dx) \quad (8)$$

Here, k_m refers to the thermal conductivity of specific medium, A_m is the cross section area of the medium and dT/dx is the temperature gradient across the length, dx. Knowing the experimental parameters of a given medium, the above equation is integrated to obtain the total axial conduction heat flow through the medium, incorporating the thermal conductivity integrals over the appropriate temperature range.

4.3.2. Regenerator ineffectiveness

The function of a regenerator is to cool the incoming gas to the refrigeration temperature by periodically transferring heat from the incoming gas to the exhausting gas through an intermediate heat exchange with the regenerator matrix. Due to the non-ideal nature, in reality, the regenerator is not 100% efficient and so, the incoming gas is not cooled to the refrigeration temperature but to a temperature slightly above it and thus a loss is introduced. The loss due to ineffectiveness of the regenerator is given as [29],

$$Q_{RG}=\dot{m}_{RG}C_PI_{RG}(T_h-T_c) \quad (9)$$

In the above equation, T_h and T_c are the temperatures of the hot and cold boundaries of the regenerator. Here I_{RG} refers to the regenerator inefficiency. The NTU method has been applied to evaluate the regenerator efficiencies down to 20 K, when the heat capacity ratio $C_r=(m_wC_w/(\dot{m}C_p\tau))$ is greater than 100 (i.e. the matrix tempera-

Table 2
Refrigeration losses by different mechanisms

Sl. No	Loss due to	$Q_{Loss}(W)$	
		Configuration 7	*Configuration 1*
1.	Axial heat conduction total	0.2263	0.6727
	(a) by working fluid, Helium gas	0.096	0.107
	(b) by walls of Pulse tube and Regenerator (2nd Stage)	0.082	0.1492
	(c) by regenerator Matrix Materials (2nd Stage)	0.0483	0.4165
2.	2nd Stage regenerator Inefficiency	6.293	7.023
3.	Pressure drop in 2nd stage regenerator		
	(a) Theoretical	1.026 ($\Delta P_{th} = 0.82 \times 10^5 Pa$)	1.105 ($\Delta P_{th} = 0.75 \times 10^5 Pa$)
	(b) Experimental	0.6009[a] ($\Delta P_{exp} = 0.48 \times 10^5 Pa$)	0.6777[a] ($\Delta P_{exp} = 0.46 \times 10^5 Pa$)
4.	Radiation to 2nd stage cold end from ambient	0.0548	0.042
	Total loss of refrigeration power	7.175[a]	8.415[a]

[a] Refrigeration loss calculated with the experimental pressure drop.

ture swing is very small) [29]. Although, this method may not directly be applicable to a 4 K regenerator, still it may be able to provide a reasonable estimate of the regenerator inefficiency and hence we have applied this for further calculation.

An expression for the regenerator efficiency based on NTU method is given by Kush et al [29] and is given below. The regenerator effectiveness, $\varepsilon_{RG} = NTU/(NTU + 1)$, and $\varepsilon_{RG} = (1 - I_{RG})$. *NTU* is given by $NTU = (\alpha A_{HT}/\dot{m}_{RG} C_p)$, where α refers to the heat transfer coefficient, A_{HT} is the heat transfer area, $\dot{m}_{RG}$ is the mass flow rate through the regenerator and C_p is the specific heat of the gas. The heat transfer coefficient α may be given by several expressions [29], of which we have chosen the one used by Wang [22] and Ju et al. [30]. Thus, α can be written as,

$$\alpha = 0.023(k/d_h)Re^{0.8}\mathrm{Pr}^{0.4} \tag{10}$$

In the above equation, the Reynolds number $Re = (\rho v d_h/\eta)$ and the Prandtl number $\mathrm{Pr} = (C_p\eta/k)$. The hydraulic diameter d_h is given as $d_h = (4 l_{RG} A_{flow}/A_{HT})$. The flow area $A_{flow} = \varphi(\pi d_{RG}^2/4)$ and the heat transfer area $A_{HT} = 6(1 - \varphi)V_{RG}/d_{RG}$ and φ is the porosity [29]. The mass flow rate in the expression for *NTU* was chosen as the cold end mass flow rate $\dot{m}_c$ through the regenerator.

4.3.3. Pressure drop in regenerator

One of the important refrigeration loss mechanisms in a cryocooler is that due to the pressure drop across the regenerators. The refrigeration loss Q_{pd} due to pressure drop is given by Thirumaleshwar et al. [28] as,

$$Q_{pd} = (\Delta P/P_{avg})[(PR + 1)/(PR - 1)]Q_i \tag{11}$$

Here, ΔP is the average pressure drop across the regenerator and P_{avg} is the average pressure in the system, PR is the pressure ratio. For a randomly stacked spherical particle matrix, the friction factor f and ΔP are given by [29],

$$f = [(1 - \varphi)/\varphi][570(1 - \varphi^2)/(\varphi Re) + 3.5] \tag{12}$$

and

$$\Delta P = f(l_{RG}/d_s)(G^2/2\rho) \tag{13}$$

Here, d_s represents the average diameter of the spherical particle in the regenerator matrix and G is the mass flow rate per unit area and is given by $G = (\dot{m}_c/A_{flow})$. Thus one can obtain ΔP and hence Q_{pd}.

Alternately, if one assumes that there is no pressure drop across the pulse tube, then the pressure drop across the regenerator can be calculated from the pressure waveforms monitored at the warm end of the first stage regenerator and the warm ends of the first and second stage pulse tubes. Both the methods have been adapted to obtain the refrigeration losses due to pressure drop.

4.3.4. Radiation heat transfer

The refrigeration loss due to radiation occurs because of the heat exchange between the walls of the vacuum enclosure at ambient and the cold end of the PTC. This radiation heat transfer is given by,

$$Q_{rad} = \frac{\sigma F A_{CX2}^{outer}(T_o^4 - T_{CX2}^4)}{(1/e_c + 1/e_h + 2/e_s - 2) + (N_S - 1)(2/e_s)} \tag{14}$$

Here σ refers to the Stefan - Boltzmann constant, N_S represents the number of insulation layers, e_s, e_c and e_h denote the emissivities of the superinsulation, cold and hot surfaces respectively. A_{CX2}^{outer} is the outer surface area of the second stage cold end heat exchanger. The view factor F is 1, when the cold surface is fully surrounded by the warm surface. In general, the refrigeration loss due to radiation is much smaller compared to the other losses.

The refrigeration power losses due to the different mechanisms discussed above have been presented in Table 2 for two specific configurations 7 and 1 under no-load conditions (i.e. the second stage cold end is at the lowest temperature). The regenerator ineffectiveness accounts for more than 80% of the total loss of refrigeration power. The axial conduction and the pressure drop contribute to the refrigeration losses, but to a smaller extent. The pressure drops in the pulse tube coolers are arrived at, both from the experimental pressure wave forms as well as by using the Eqs. (12) and (13). It is observed that they are of the same order of magnitude. The refrigeration loss due to radiation heat transfer is found to be the least. The above refrigeration loss data is used in the following section to compare the experimentally measured refrigeration powers with the theoretical predictions of the models.

5. Comparison of experimental results with theoretical models

5.1. Refrigeration power

Similar to the observations of Zhu et al. [19] and Wang [22], both the models predict higher mass flow rates at the cold end than those at the warm end. The theoretical predictions of the refrigeration powers by both the models have been attempted for two specific configurations of PTCs, namely 7 and 1 (in Table 1). Figs. 8(a) and (b) compare the theoretical values of refrigeration powers using the isothermal model with the experimental values for the second stage for Pulse tube coolers of configurations 7 and 1 respectively. It is observed that the theoretical values (with the losses subtracted) are quite high and at least an order of magnitude higher than the experimental data. This is understandable, since isothermal model does not take into account of the real gas effects of the working fluid close to its liquefaction temperature.

Fig. 9(a) compares the experimental refrigeration powers of PTC, configuration 7, with those predicted by the energy equation

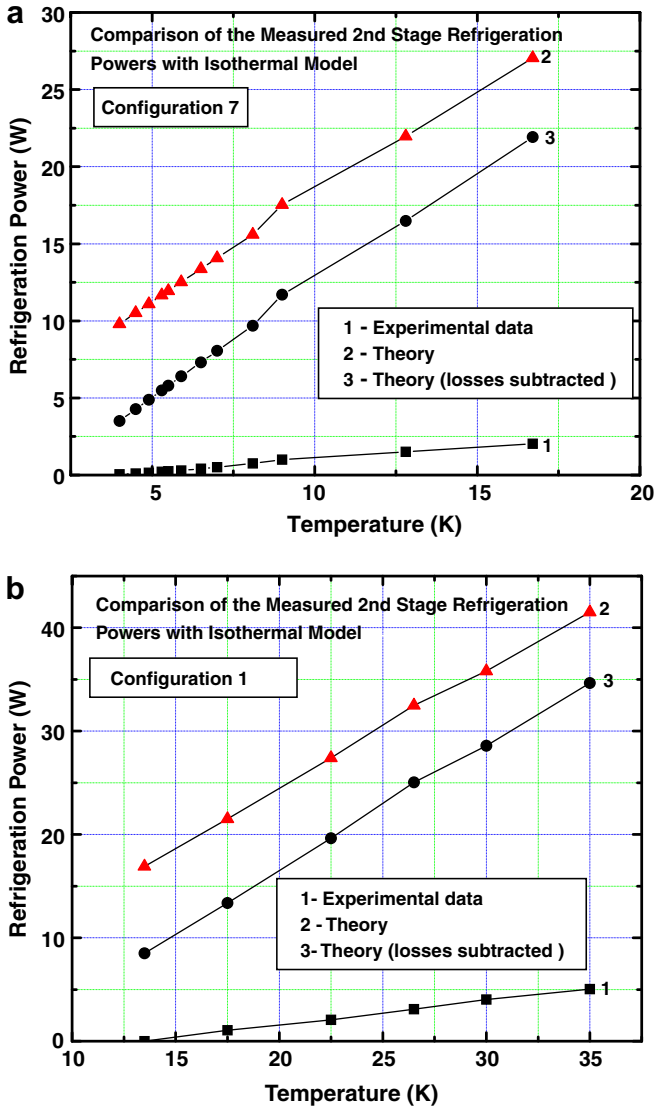

Fig. 8. (a) Comparison of the measured 2nd Stage refrigeration powers with isothermal model for PTC, configuration 7. (b) Comparison of the measured 2nd Stage refrigeration powers with isothermal model for PTC, configuration 1.

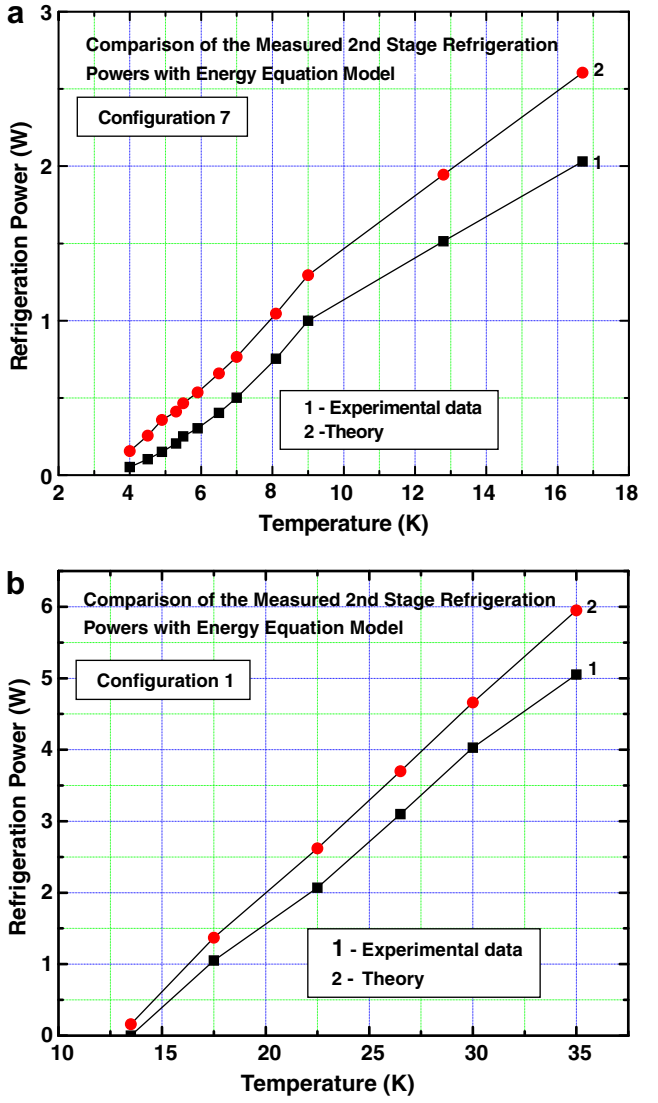

Fig. 9. (a) Comparison of the measured 2nd Stage refrigeration powers with energy equation model for PTC, configuration 7. (b) Comparison of the measured 2nd Stage refrigeration powers with energy equation model for PTC, configuration 1.

model. The above model predicts an enthalpy flow rate through the regenerator, $\dot{h}_{RG} \sim 6.55$ W at 4 K, which is quite comparable with the refrigeration loss by regenerator inefficiency, namely 6.293 W (in Table 2). Since the enthalpy flow rate through pulse tube is predicted as $\dot{h}_{PT} \sim 6.705$ W at 4 K, a refrigeration power of $\sim$ 0.155 W is expected at this temperature. It is seen from the figure that the experimental refrigeration powers are somewhat lower than the theoretical predictions. Fig. 9(b) presents similar results for the PTC, configuration 1. In this case, the model predicts $\dot{h}_{RG}$ to be $\sim$7.73 W. This value also matches fairly well with the regenerator inefficiency loss given in Table 2, namely 7.023 W. Similar to configuration 7, the theoretical refrigeration powers are higher than the experimental values and the deviation becomes larger at higher temperatures. From the above, it is clear that the energy equation model leads to a better prediction of refrigeration powers than the isothermal model.

5.2. Pulse tube wall temperature profiles

In the isothermal model, the pulse tube is divided into only three control volumes. Hence, the prediction of the pulse tube wall temperature profiles by this model is difficult, and hence this model has not been used for this purpose. On the other hand, the energy equation model discretizes the pulse tube / regenerator system into a large number of elements (control volumes) and leads to the prediction of pulse tube wall temperature profile. Fig. 10 compares the theoretically predicted temperature profiles with that of the experimental data for configurations 7 and 1, along with the experimental data from [22]. It can be seen that there is a good agreement between the experimental data and the theoretical temperature profiles.

6. Conclusion

In this work, several configurations of two stage pulse tube Cryocoolers have been experimentally studied, by varying the dimensions of pulse tubes and regenerators (of both stages) as well as by modifications of regenerator materials for the second stage to arrive at the best configuration (the one with the lowest second stage cold end temperature). The PTC, configuration 7 produces a no-load temperature of $\sim$3 K and gives a refrigeration power of $\sim$250 mW at 5 K. This system uses meshes of stainless steel along

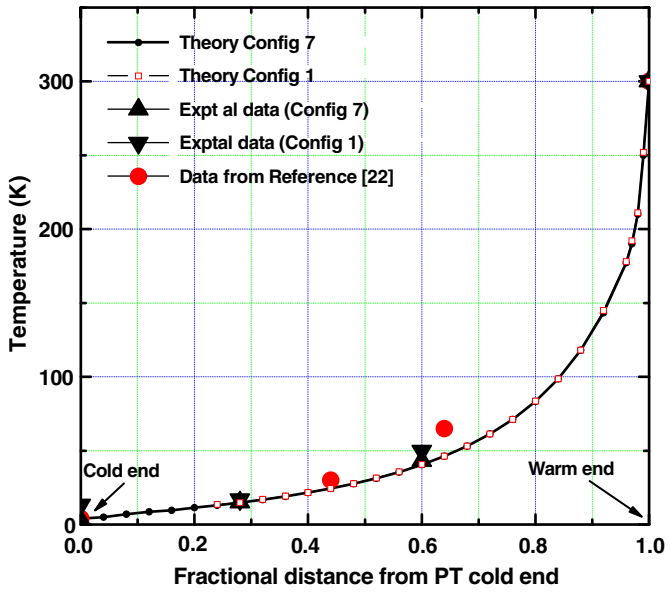

Fig. 10. Comparison of theoretical and experimental temperature profiles on pulse tube. Data from the reference [22] is also included.

with Pb for the first stage regenerator and $HoCu_2$, Er_3Ni, Pb, and SS meshes in the volume percentage ratio 27:27:27:19 for the second stage regenerator. Experimental results show that the configuration, which leads to the lowest temperature, is not necessarily the one which gives the highest refrigeration power at a given temperature.

The studies indicate the need for magnetic materials such as Er_3Ni, $HoCu_2$ along with Pb for the second stage regenerator to achieve temperatures below 10 K. Detailed experimental studies have been conducted by varying the volume percentage ratios of Er_3Ni to Pb and $HoCu_2$ to Pb in PTC, configuration 7. The systems with $HoCu_2$ performed better than those with Er_3Ni. The results show that for the best performance of PTCs, the optimum volume percentage ratios should be 40:60 in the case of $HoCu_2$ to Pb. The same ratio should be 60:40 for the case of Er_3Ni to Pb.

The theoretical analysis of PTC has been carried out by using both the isothermal model as well as the energy equation model. The predicted refrigeration powers (after taking into account of the important loss mechanisms) have been compared with the experimental results for two specific pulse tube configurations 7 and 1. The predicted refrigeration powers by the isothermal model after the important loss mechanisms are considered are quite deviated from the experimental values. On the other hand, the refrigeration powers predicted by the energy equation model are quite comparable with the experimental values. However, in all cases, the experimentally measured refrigeration powers are always lower than the theoretical predictions. It is also observed that the pulse tube temperature profiles predicted by the energy equation model compare quite well with the experimentally measured values.

Acknowledgements

The authors acknowledge the financial support from the Council of Scientific and Industrial Research (CSIR), New Delhi, India, towards a project on the development of a multistage pulse tube Cryocooler, which enabled the research in this area. The authors are also thankful to the staff of Centre for Cryogenic Technology, Indian Institute of Science, for their valuable help in the design and fabrication of the experimental systems.

References

[1] W.E. Gifford, R.C. Longsworth, Pulse tube Refrigeration, Trans. ASME J. Eng. Industry 86 (1964) 264–268.
[2] E.I. Mikulin, A.A. Tarasov, M.P. Shkrebyonock, Low temperature expansion pulse tubes, Adv. Cryog. Eng. 29 (1984) 629–637.
[3] R. Radebaugh, J. Zimmerman, D.R. Smith, B. Louie, A comparison of three types of pulse tube refrigerators: new methods for reaching 60 K, Adv. Cryog. Eng. 31 (1986) 779–789.
[4] S. Zhu, P. Wu, Z. Chen, Double inlet pulse tube refrigerator: an important improvement, Cryogenics 30 (1990) 514–520.
[5] A. Ravex, P. Rolland, J. Liang, Experimental study and modelisation of a pulse tube refrigerator, Cryogenics 32 (1992) 9–12.
[6] T. Hasimoto, M. Ogawa, A. Hayashi, Recent progress on rare earth magnetic regenerator materials, Adv. Cryog. Eng. 37 (1992) 859–865.
[7] L.M. Qiu, Y.L. He, Z.H. Gau, G.B. Chen, A single stage pulse tube cooler reached 12.6 K, Cryogenics 45 (2005) 641–643.
[8] Y. Matsubara, J. Gao, Novel Configurations of 3 stage pulse tube Refrigerator for temperatures below 4 K, Cryogenics 34 (1994) 259–262.
[9] C. Wang, G. Thummes, C. Heiden, A two stage pulse tube cooler operating below 4 K, Cryogenics 37 (1997) 159–164.
[10] G. Thummes, S. Bender, C. Heiden, Approaching the He^4 λ – line with liquid nitrogen precooled two-stage pulse tube refrigerator, Cryogenics 36 (1996) 709–711.
[11] J. Gao, Y. Matsubara, Experimental Investigations of 4 K pulse tube refrigerator, Cryogenics 34 (1994) 25–30.
[12] M.Y. Xu, A.T. A.M. De Waele, Y.L. Ju, A pulse tube refrigerator below 2 K, Cryogenics 39 (1999) 865–869.
[13] C. Wang, Helium liquefaction with a 4 K pulse tube cryocooler, Cryogenics 41 (2001) 491–496.
[14] N. Jiang, U. Lindemann, F. Giebeler, G. Thummes, A He^3 pulse tube cooler operating down to 1.3 K, Cryogenics 44 (2004) 809–816.
[15] C. Wang, P. Gifford, Development of 4 K pulse tube refrigerators at cryomech, Adv. Cryog. Eng. 47 (2002) 641–648.
[16] J.L. Gao, IGC-APD advanced two-stage pulse tube cryocoolers, Adv. Cryog. Eng. 47 (2002) 683–690.
[17] Ray Radebaugh, A review of pulse tube refrigeration, Adv. Cryog. Eng. 35 (1990) 1191–1205.
[18] P.C.T. Boer, Thermodynamic analysis of the basic pulse tube refrigerator, Cryogenics 34 (1994) 699–711.
[19] S. Zhu, Z. Chen, Isothermal model of the pulse tube refrigerator, Cryogenics 34 (1994) 591–595.
[20] C. Wang, P. Wu, Z. Chen, Numerical modeling of an orifice pulse tube refrigerator, Cryogenics 32 (1992) 785–790.
[21] J. Liang, A. Ravex, P. Rolland, Study of pulse tube refrigeration. Part 1: Thermodynamic nonsymmetry effect cryogenics 36 (1996) 87–93; J. Liang, A. Ravex, P. Rolland, Study of pulse tube refrigeration. Part2. Theoretical modeling, Cryogenics 36 (1996) 95–99; J. Liang, A. Ravex, P. Rolland, Study of pulse tube refrigeration. Part3: Experimental verification, Cryogenics 36 (1996) 101 – 106.
[22] C. Wang, Numerical analysis of the 4 K pulse tube coolers. Part I: Numerical simulation, Cryogenics 37 (1997) 207–213; C. Wang, Numerical analysis of the 4 K pulse tube coolers. Part II: Performances and internal processes, Cryogenics 37 (1997) 215–220.
[23] A. Hofmann, H. Pan, Phase shifting in pulse tube refrigeration, Cryogenics 39 (1999) 529–537.
[24] C. Wang, Y.L. Ju, Y. Zhou, The experimental investigations of a two-stage pulse tube refrigerator, Cryogenics 36 (1996) 605–609.
[25] S. Wild, L.R. Oellrich, A. Hofmann, Two Stage Double Inlet Pulse Tube Refrigerator Down to 10 K, Cryocoolers 9 (1997) 255–260.
[26] J. Yuyama, M. Kasuya, Experimental study on refrigeration losses in pulse tube refrigerators, Cryogenics 33 (1993) 947–950.
[27] Y.L. Ju, On the heat conduction losses of Pulse tube and Regenerator at temperature range of 300–4 K, Adv. Cryog. Eng. 47 (2002) 942–949.
[28] M. Thirumaleshwar, S.V. Subramanyam, Gifford McMahon cycle – a theoretical analysis, Cryogenics 26 (1986) 177–188.
[29] P.K. Kush, M. Thirumaleshwar, Design of regenerators for a GM cycle refrigerator, Cryogenics 29 (1989) 1084–1091.
[30] Y.L. Ju, C. Wang, Y. Zhou, Numerical simulation and experimental verification of oscillating flow in pulse tube refrigerator, Cryogenics 38 (1998) 169–176.